Mechanical properties of a staghorn coral skeleton, *Acropora cervicornis*

Douglas Steinbach

Department of Mechanical and Aerospace Engineering, Herbert Wertheim College of Engineering, University of Florida

Abstract

The art of using nature to create objects for human use is popular through tree shaping (also called Arbortecture or Pooktre). It is possible that the manipulation of coral growth could also build practical structures. Before building structures of coral it is important to understand the mechanical properties of coral. It is necessary to understand the mechanical properties of the skeleton (aragonite) of *Acropora cervicornis* (commonly staghorn coral). This study measured the density, and quasi-static and dynamic compressive yield strength of bleached staghorn coral. Samples were taken from different parts of the staghorn coral, resulting in different cross-sections but assumed to be perfectly cylinderical and therefore leading to variation in fracture strengths. The average density was found to be 3.13 g/cm^3, and the average quasi-static fracture strength was found to be 8.56 ± 2.96 MPa. The average dynamic fracture was found to be 20.80 ± 4.96 MPa. The large scatter in the results was attributed to variation in porosity distribution and the orientation of the cylinder with respect to the growth axis. It is recommended that more systemmatic specimen extraction procedures may be employed to obtain a more accurate strength of the corals.

1.0 Introduction

Material selection has always been a major factor in mechanical engineering design. In recent years, many engineers and designers have looked to nature for inspiration and novel solutions to problems [1-2]. A famous example is Antoni Gaudi, an architect and engineer, who designed Sagrada Familia in Barcelona, a building where nature inspired the "structures, form, and geometries" [3]. A common practice for designing gardens and furniture is tree shaping (sometimes called Arbotecture or Poketre), which has recently been used to create more sustainable and green building initiatives [4]. This process involves directing the tree growth using tools dependent upon what tree is being shaped [5]. Knowing that humans can manipulate live trees, it is worth exploring if the same can be done to coral. Coral may be a material of the future or the inspiration for future manufactured materials.

Numerous coral species grow in the marine waters surrounding Florida, as the coral *Accropora cervicornis* grows it deposits aragonite (calcium carbonate $CaCO_3$). A surge in aragonite in this region and the Caribbean is due to the *A. cervicornis* coral that grows in these shallow waters [6]. *A. cervicornis* is very abundant around Florida due to its ability to fragment, where the coral breaks off from the reef and begins to grow wherever it settles, to form new reefs. The *A. cervicornis* is now listed as critically endangered [6] leading to massive reefs of bleached aragonite being left behind from the dead coral. Bleaching is the term for coral that is killed due to environmental changes that are not conducive to coral life. This coral bleaching is due to climate change [7-9]. *A. cervicornis*, however, is being grown in nurseries to be reintroduced into its natural habitat [6]. It is possible to experiment with coral shaping in these nurseries.

Before shaping coral, it is important to understand the aragonite that makes up the *A. cervicornis* skeleton. An understanding of the mechanical properties of the skeleton of *A. cer*vicornis can

help identify potential future uses of the coral. The current thesis focuses on understanding the mechanical properties of this coral through density measurements and compression testing.

The mechanical properties of *A. palmate,* a relative of *A. cervicornis,* have been documented before [10] but there is no published work on *A. cervicornis.* The porosity and microstructure of *A. cervicornis* have been characterized [11-15]. One of the natural predators of *A. cervironis* is *Hermodice carunculata* or commonly referred to as a bearded fire worm [16].

1.1 Research Objectives

The objective of this research is to determine the static and dynamic compressive strength of *A. cervicornis* aragonite skeletons. The knowledge of *A. cerviornis* skeletons of aragonite mechanical properties can shed light on its current health and potential future problems it may face in coastal regions, as more coral is bleached due to ocean acidification. The knowledge of these mechanical properties can also influence material selection and manufacturing of new future materials.

2.0 Methods

2.1 Density Measurement

The bleached *A. cervironis* was supplied by a researcher at the University of Central Florida (UCF; Orlando, FL) as six cylindrical samples of average dimensions 8.88 mm diameter x 24.37 mm height. The difference between the samples is the section from which each sample is cut from. The coral grows in branching angles, so the growth axis and diameter vary between samples. The coral was grown in a nursery in Broward County, Florida. A typical test specimen is shown in Figure 1. As noted, the specimen does not have an exact cylindrical shape but has spikes on the circumferential surface. Hence, the specimen diameter was measured by placing

dial calipers in between the spikes to measure the diameter of the circle that the spikes branch off from. This diameter measurement is highlighted in Figure 2. The sample nomenclature was given from the professor at UCF.

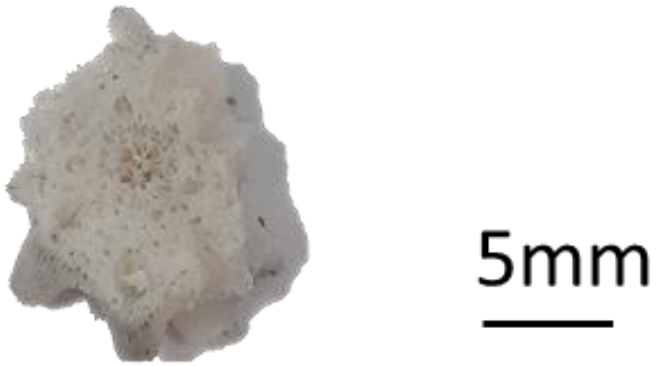

Figure 1. Sample of coral. The high porosity can be seen in the cross section. There are also spikes coming off the sides.

It can be observed in Figure 1, that the coral has a high level of porosity. This high level of porosity is a natural defense to crack propagation. As moving water stresses the coral, cracks begin to form at holes, however, neighboring holes in the structure prevent extensive crack growth, as the porosity absorbs propagating cracks. The bulk and apparent density of each sample was measured. A helium pycnometer was used to measure the apparent density of the material that comprises the specimen. A helium pycnometer relies on filling a reference chamber with helium to a chosen pressure while the sample is in another chamber that is separated by a valve. The helium is then shared between the two chambers and the pressure drop as the helium disperses is used to calculate the volume [17]. This density calculation is different from that measured by Archimedes method as the helium pycnometer relies on helium to fill up the porous volume to measure the true density of the sample material. The Archimedes method uses the dry

and wet mass of the sample (the object mass is determined while submerged in a fluid) and the density (ρ) of the fluid to measure the sample bulk density equation (1) [18]. Water was used to find the density using the Archimedes method. The Archimedes method measures the bulk density as it relies on the volume of water displaced and due to surface tension not all of the air can be removed while submerged in water. Since helium has smaller molecules than water it can penetrate smaller pores in the material. First, the mass of each specimen was measured with a scale then the volume of space the sample occupied was measured. The density of each sample and other pertinent information can be found in Table 1 below.

$$\rho_{sample} = \frac{dry\ mass * \rho_{water}}{dry\ mass - wet\ mass} \quad (1)$$

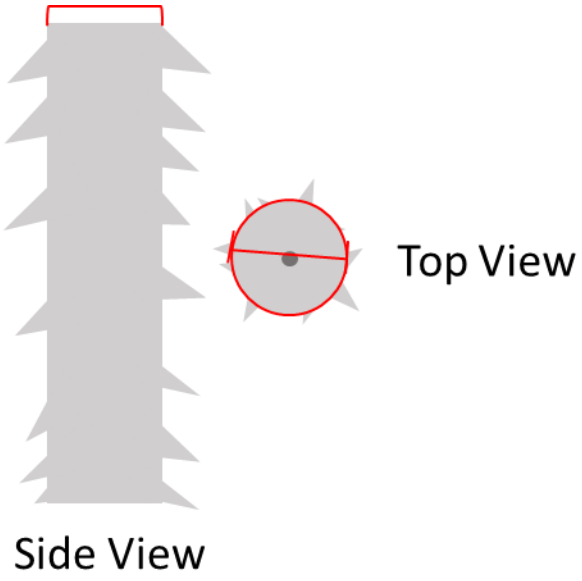

Figure 2. An image of the coral and how the diameter was measured. The diameter of the inner circle was used as the diameter of the sample for stress calculations.

Table 1. *Coral Samples, the codes given to the differing samples and the size and mass of the samples.*

Sample	Length (mm)	Diameter (mm)	Mass (g)	Volume (He) (cm^3)	Density (g/cm^3) (He)	Density (g/cm^3) (Arch)
1 Bleached a (1B a)	27.73	11.22	4.58	1.40±0.04	3.27	2.56
1 Bleached b (1B b)	27.13	8.17	2.92	1.18±0.03	2.47	2.72
3 Sanded f (3S.f)	20.53	9.89	2.95	0.88±0.02	3.35	2.55
3 Sanded g (3S.g)	22.02	7.94	2.04	0.56±0.01	3.64	2.52
4 Bleached a (4B a)	25.59	8.16	1.78	0.56±0.01	3.18	2.61
4 Bleached b (4B b)	23.23	7.87	1.75	0.55±0.01	3.20	2.62

The names for the differing samples was predetermined by the researcher from UCF. The name dictates samples being cut from different segments of the coral.

2.2 Sample Preparation

Initial efforts were made to measure longitudinal and shear wave velocities in these samples using pulse echo ultrasonic technique, with intent to determine their elastic properties (Young's modulus and Poisson's ratio). However, due to the high level of porosity in each sample, no wave reflections were observed and hence the method was abandoned. The samples were cut into smaller lengths using an Allied High Tech Products, Inc. Techcut 4™ precision low speed saw with a diamond blade for compression testing. The dimensions of the samples averaged were 5.53 mm in length x 8.68 mm in diameter. The cut surfaces were not parallel to each other and so samples were sanded down using 300 grit sanding paper. No attempt was made to measure the parallelism of the loading surfaces.

Both static and dynamic compression tests were performed on these specimens. The static tests were conducted using a Test Resources® Model 311 Frame machine at a displacement rate that varied between each sample as it was calculated using equation (2) of an average $5.67*10^{-3}$

mm/s, resulting in a deformation strain rate of 10^{-3} s^{-1}. Dynamic compression tests were conducted at a strain rate of 10^{2} s^{-1} in a Split Hopkinson Pressure Bars (SHPB). Multiple tests were conducted to capture the influence of wide range of microstructural heterogeneities and porosity distributions.

2.3 Quasi-static Compression

In quasi-static compression the load is applied slowly on the specimen resulting in a strain rate ($\dot{\varepsilon}$) on the order of 10^{-3} s^{-1} [20]. The specimen is held between the two loading columns in the test machine and one of the columns is slowly moved thus compressing the specimen. The load was measured by a load cell on top of the upper column and the displacement of the column was measured by a digital position encoder. Both these quantities are monitored to obtain the load-displacement (or stress-strain) curve for the material.

Thirteen samples were tested in quasi-static compression. The strain rate was chosen to be 10^{-3} s^{-1} and this was used to calculate the velocity of the loading column in the compression machine as per,

$$v = l_0 \times \dot{\varepsilon} \tag{2}$$

where v is the velocity of the sample, l_0 is the original length of the sample, and $\dot{\varepsilon}$ is the strain rate the sample. The quasi-static test setup can be seen below in Figure 3. It consisted of two parallel platens faces, with a load cell connected to the top platen, that apply force to the sample.

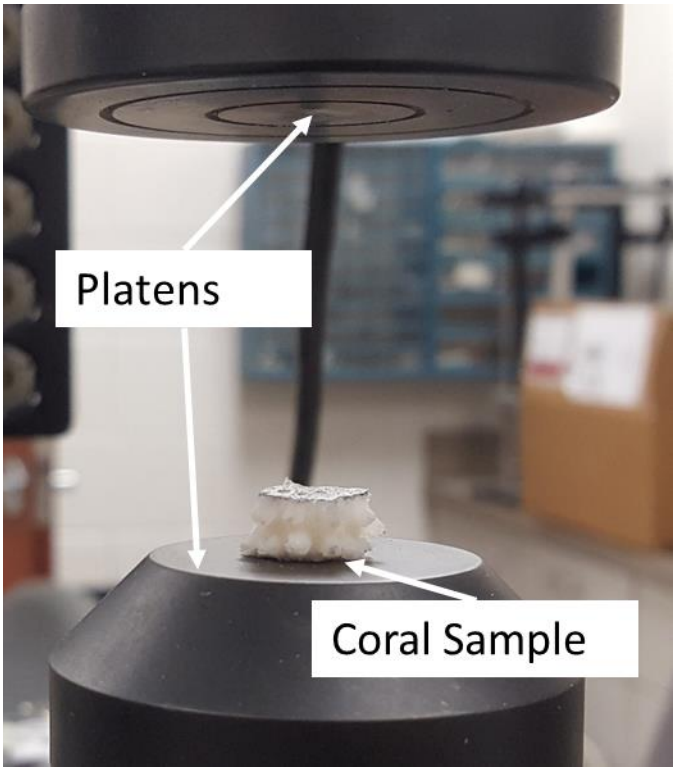

Figure 3. Experimental set up of the Quasi Static compression test.

2.4 Dynamic Compression

A Split Hopkinson Pressure Bar (SHPB) assembly is commonly used to determine dynamic compressive strength of a material. The assembly consists of a set of long slender bars of the same material and diameter (maraging steel of 12.7mm diameter for this investigation) [21-22], as shown schematically in Figure 4. The bars must be the same material and diameter to be impedance equation (3) matched. Impedance is the density (ρ), cross sectional area (A), and wave velocity (C) of the material multiplied together. A striker was launched from a gas gun, which impacts an incident bar. This impact sends a compressive pulse down the incident bar that was measured by a strain gage and the compressive pulse continues through the transmission bar that also has a strain gage. A sample was placed in between the incident and transmission bars.

This sample was subjected to high strain rate deformations depending on the gas gun pressure that was used to accelerate the striker bar. Upon reaching the sample, the pulse causes deformation and abrupt failure of the sample. The compressive wave that fails the sample continues into the transmission bar, the remainder of the pulse is reflected in tension into the incident bar. In a standard SHPB, due to the flat surfaces of the striker and incident bars, a square pulse is generated upon impact. A thin copper disk placed between the striker and incident bars generates a triangular pulse, which yields a constant strain rate during the elastic deformation of the specimen. This ramped load is preferred for testing of brittle samples [22].

$$impedance = \rho CA \tag{3}$$

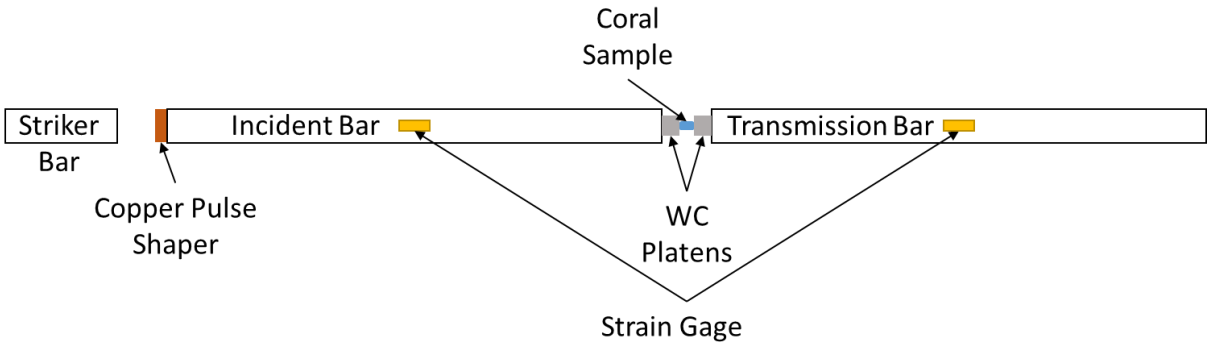

Figure 4. Standard SHPB set up schematic. The strain gages collect all the data in this set up.

The peak of the compressive wave that is registered in the transmitted bar is used to find the stress in the sample. The peak of the reflected tension wave in the incident bar is used to find the strain rate and strain of the sample. This strain in the incident bar is used to find the strain rate

(4). Where ε_{bar} is the strain in the incident bar, C_{bar} is the velocity of a wave in steel, and L_{sample} is the length of the sample.

$$\dot{\varepsilon} = \frac{2\varepsilon_{bar}C_{bar}}{L_{sample}} \tag{4}$$

With the strain rate (which is the same in the bar and sample) the strain induced upon the sample can be calculated using the trapezoidal rule.

The stress induced upon the sample is calculated using (5). The strain ε_{Tbar} is from the transmitted bar in this equation, the area of the bar is A_{bar}, E_{bar} is the modulus of elasticity of the steel bar, and A_{sample} is the area of the sample.

$$\sigma = \frac{-\varepsilon_{Tbar}A_{bar}E_{bar}}{A_{sample}} \tag{5}$$

Samples with poor impedance matching or large porosity can have trouble transmitting the compressive wave. The poor impedance matching leads to the compressive wave fracturing the sample without the wave reaching the transmission bar. The compressive wave does not travel through air so large porosity leads to the sample having poor impedance even if the overall cross-sectional area of the sample is large. The data of one of the coral samples tested in the SHPB is shown in Figure 5. With no transmission signal above the noise level the stress cannot be calculated with any certainty.

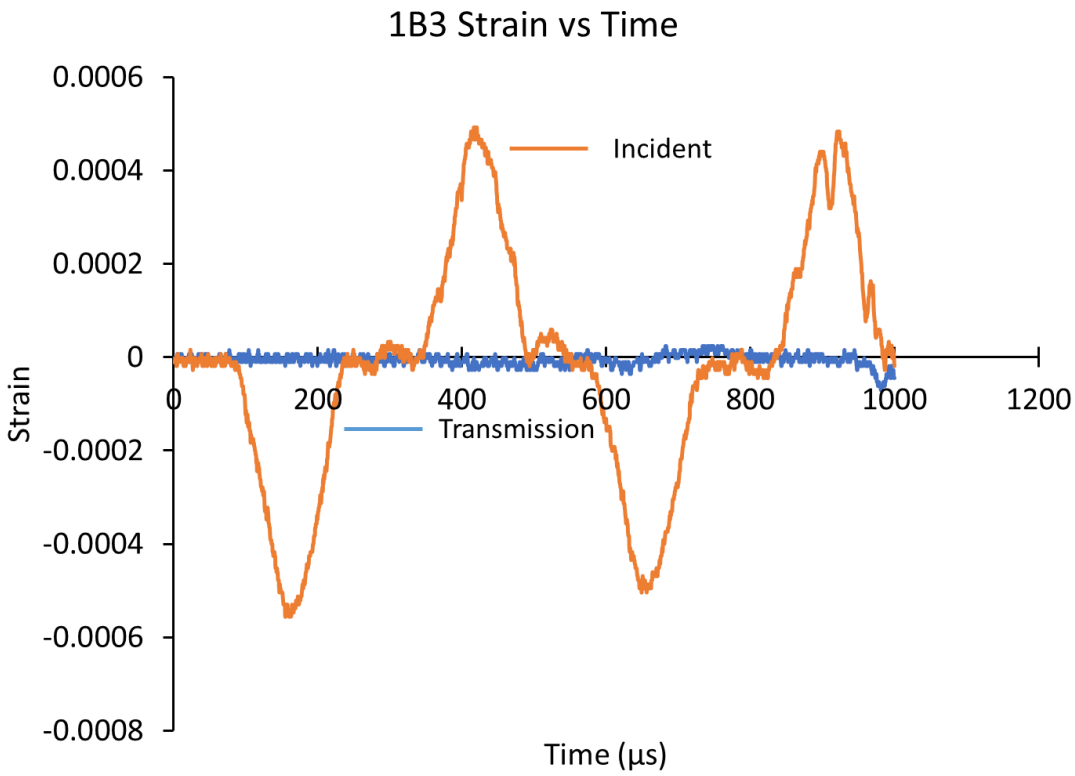

Figure 5. Sample 1B b3 was tested without the load cell. It can be seen that the transmission signal never leaves the noise level.

To combat the lack of signal, a load cell was placed between the bars to register the load at which the sample fails. This new set up with a load cell allows the strain rate to be calculated from the reflected incident signal with equation (4) and the stress to be calculated with equation (6). Tungsten Carbide (WC) platens are placed between the incident and transmission bars to protect the bar from damage, as they are much harder than the steel but softer than the coral being tested. A sample being tested is placed in between the WC platens. A schematic of the test setup may be found in Figure 6. The signal the load cell provides in conjunction with the incident bar signal is shown in Figure 7. Plastic holders are used to hold the WC platens and load cell in place. Without the plastic holders, the load cell and WC can be damaged. A schematic of the test system is shown in Figure 8. The remaining six samples were tested in this manner.

$$\sigma = \frac{F}{A} \tag{6}$$

The load cell gives a voltage that needs to be multiplied by 1000 to get the force induced on the load cell. With this load, the uniaxial compressive stress is calculated using equation (6). Where F is the force from the load cell and A is the area of the sample. An example of the signal from the incident bar and load cell can be seen in Figure 7.

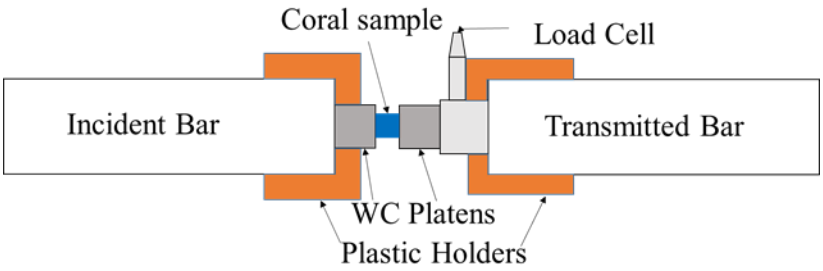

Figure 6. Schematic of the SHPB set up with a load cell.

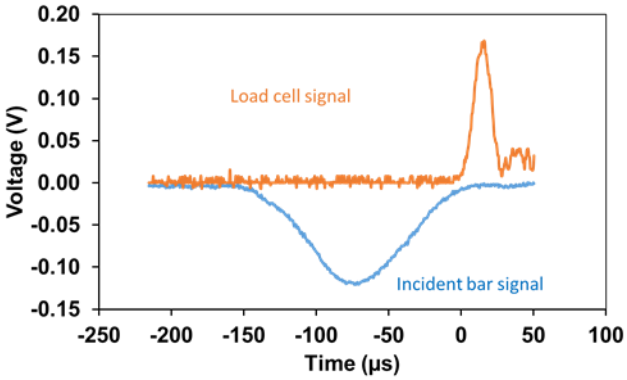

Figure 7. Example signal using the load cell on the SHPB. The incident bar signal is the same as the standard SHPB set up.

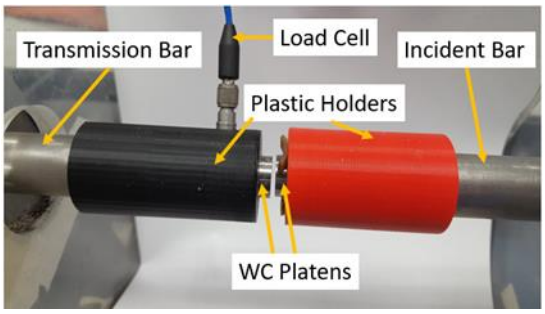

Figure 8. Experimental setup of the SHPB with the load cell.

3.0 Results & Discussion

3.1 Density

The density measurements gave varying results. This is likely due to the large variation in pore shape, size and porosity distribution in the coral microstructure of each sample. The He pycnometer volume was measured five times for each sample and there was a trend of the volume decreasing after each volume measurement. This trend is likely due to air in the samples slowly being displaced that was trapped in the samples. The variable porosity led to the different densities between each sample. Compared to the reported density of aragonite, which is 2.93 g/cm^3 [19] this study found an average density of 3.19 g/cm^3, which was 8.8% greater than the literature. There was also an outlier in the densities found in this study. The 1B b coral had a density of 2.47g/cm^3, which was over two standard deviations from the mean. Excluding the outlier, the difference between the literature and this study is 13.6% greater (3.33 g/cm^3).

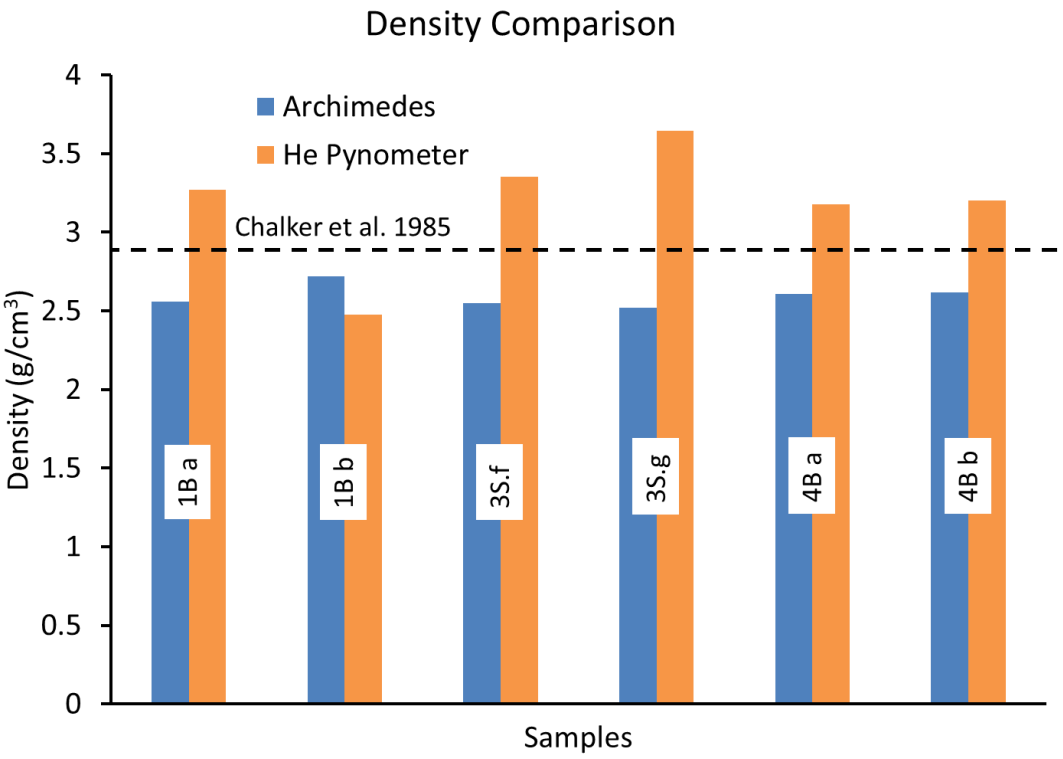

Figure 9. The density measurements of the two different methods with the literature density overlaid.

3.2 Quasi-static

The quasi-static stress-strain curves below show the varied strength of the samples taken from different parts of the coral. Strain at failure was found to be highly variable for most samples. This result is likely due to two reasons: (i) the porosity level varied from one sample to another and (ii) the specimen surfaces not being perfectly flat and parallel to each other. However, some of the graphs had very similar strains and failures, such as the 1 Bleached samples and 4 Bleached a. The peaks denoted as failure were close to each other in stress and in strain.

The stress-strain curves show many steps of sudden load drops (unloading) while testing the coral. These steps are expected due to the high level of porosity in the samples [23-25]. As the

load increases, stress concentrations occur at the pores and cause branches to fracture. Once a branch cracks, the crack will propagate until it reaches the next pore. The coral evolved a defense against failure by creating all these pores in the structure. Effectively, the pores act as a natural barrier to crack propagation. Once the load has increased too greatly the pores can no longer prevent failure, and the coral crumbles.

All the plots of stress-strain follow the same trend of stress build up then unloading steps from cracks forming and propagating to nearby pores. The differences in failure between samples cut from the same section is likely due to imperfect sanding and micro cracking. The difference between sample types is likely due to the orientation of the microstructure. As mentioned earlier, the coral grows at an angle so cutting two parallel flat surfaces will lead to the microstructure being at an angle relative to a regular cylinder. Figure 10 shows a coral branch, and how a sample can be cut from it in two different ways to ensure parallel faces. The different possibilities of cuts can be seen representatively in Figure 11. Figure 11 highlights what these samples look like when cut from the different orientations. Included are exaggerated images of the coral having varying diameter along the length of the coral. The growth angle will vary between samples cut from different sections of the coral. It is likely that this variation in angle of the microstructure axis leads to variability in the mechanical properties during this study.

As *A. cervicornis* grows, it branches out at different angles to form the staghorn shape. Therefore, cutting samples from different locations lead to the cut pieces being at different angles. Once the loading surfaces of these pieces are polished to be flat and almost parallel to each other, the coral will have the microstructure at an angle relative to the axis of the cylinder. Hence, each coral may be slightly different in its microstructure orientation with respect to its

axis. This variation in microstructure will lead to variation in the strength measured in quasi-static and dynamic compression.

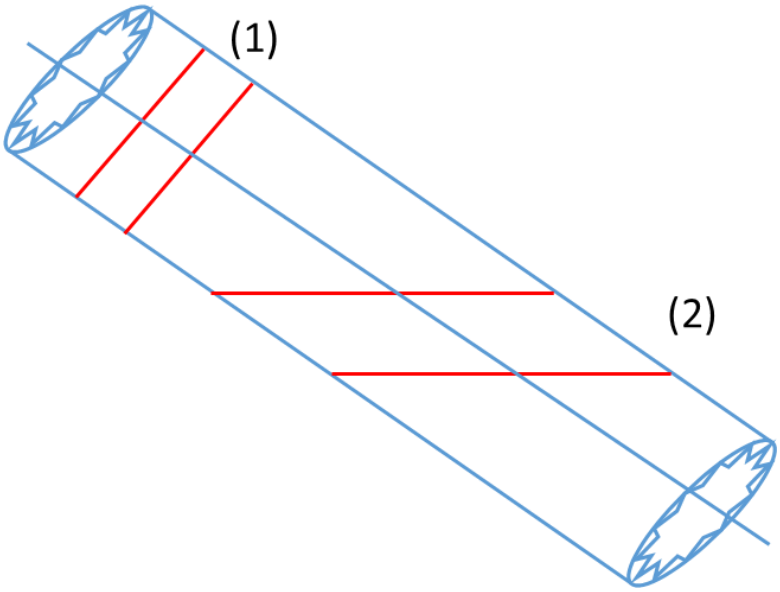

Figure 10. A representation of a piece of coral that grows at an angle. The red lines at (1) show coral being cut perpendicular to the angle of the coral. The red lines at (2) show coral being cut with lines that are parallel but at an angle to the coral.

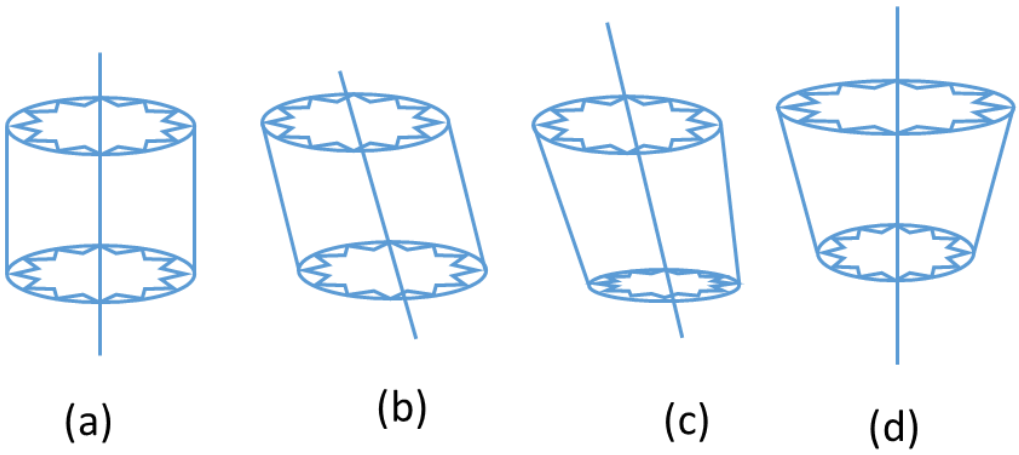

Figure 11. (a) and (d) show coral cut from (1). (b) and (c) show coral cut from (2). (c) and (d) are exaggerated to show how the diameter varies.

Table 2 shows that the stress at failure was not highly variable except for the final sample. The high variability in the 4B b samples likely stems from the uneven faces. The final sample tested was 4B b4. The test was set to travel twice the distance as normal (1mm in distance as opposed to 0.5mm) as is shown in larger strain in Figure 17. It is possible the increased distance influenced the stress allowing it to increase. It is more likely that the lack of parallelism led to the different stress.

The 12 samples originally tested were all run until the machine compressed the sample a total of 0.5mm. Figure 12 shows both the samples having dips from the porosity of the samples protecting the coral from failure. The failure was determined to be when the samples reached similar peaks, albeit at different strains. Figure 13 shows the 1B b samples peaking at similar strains and stresses so this was determined to be failure. Figure 14 shows sample 3S.f where one sample fractured quickly at a large strain rate and the 3S.f2 sample slowly climbed with a peak towards the end. The 3S.g samples shown in Figure 15 behaved differently but both had peaks towards the lower strains so it was assumed the sample failed early. The samples cut from the 4B a sample shown in Figure 16 both had peaks that overlaid each other in both stress and in strain, and the failure was determined to be at this point. Lastly, Figure 17 with 4B b samples had two similar tests between the first and two samples but the final sample tested for a longer period had a higher stress at failure and a higher strain.

The variable stresses are likely due to the orientation of the specimens as noted in Figure 11. Coral cut in different orientations may act as a fiber composite at an angle relative to the applied load. It was also not possible to check the samples to ensure exactly parallel faces, which could lead to variable strengths. It is possible since the samples had non-parallel faces it would have been more beneficial to run each test for longer.

Table 2. Quasi Static samples dimensions and results.

Sample	Area (mm^2)	Force (N)	Stress (MPa)
1B a	97.28±14.17	456.0±70.43	4.68±0.04
1B b	53.36±1.15	413.7±2.54	7.76±0.12
3S.f	69.58±2.82	775.9±19.09	6.26±0.18
3S.g	47.76±1.24	216.1±34.56	4.55±0.84
4B a	42.37±2.93	523.2±20.24	7.24±0.38
4B b	45.53±4.27	484.9±91.68	10.84±2.82

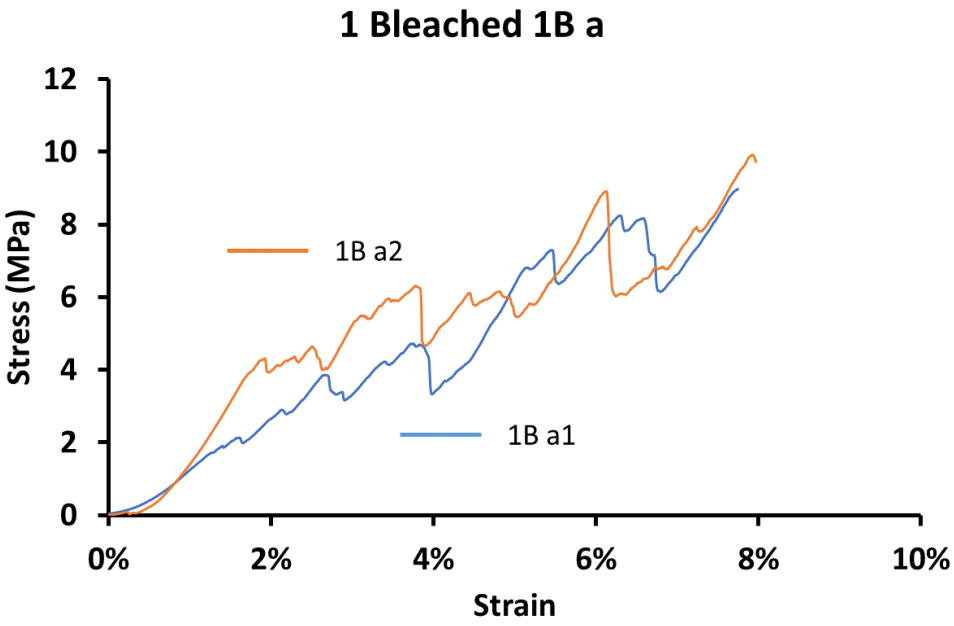

Figure 12. Quasi Static results of the bleached 1B a samples.

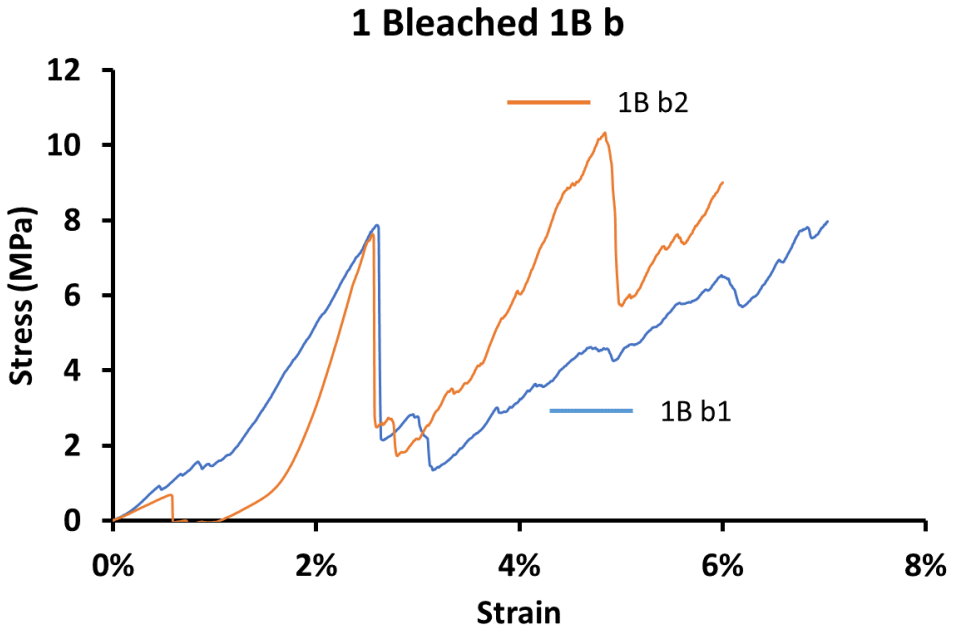

Figure 13. The Quasi Static results of the 1 Bleached 1B b samples.

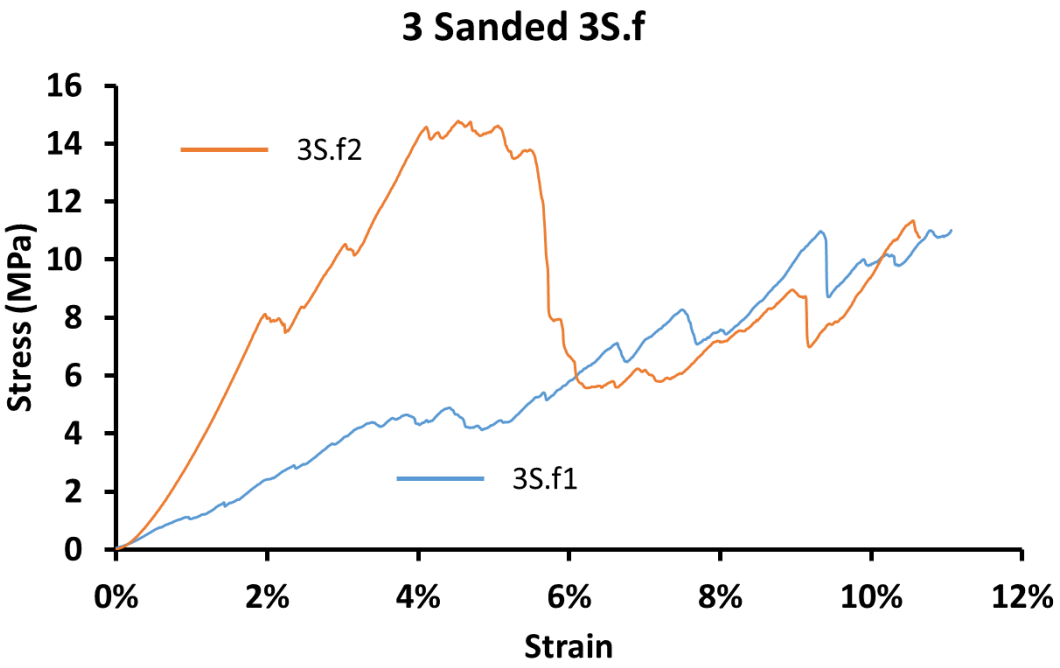

Figure 14. The Quasi Static result of the 3 Sanded 3S.f samples.

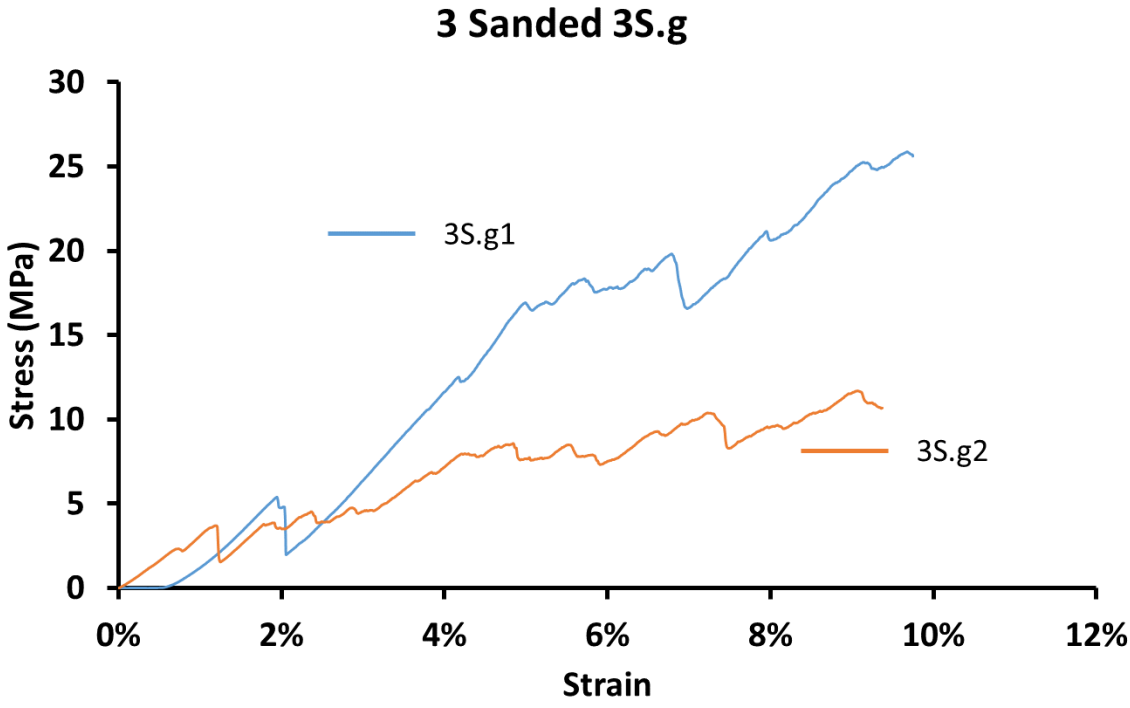

Figure 15. The Quasi static result of the 3 Sanded 3S.g samples.

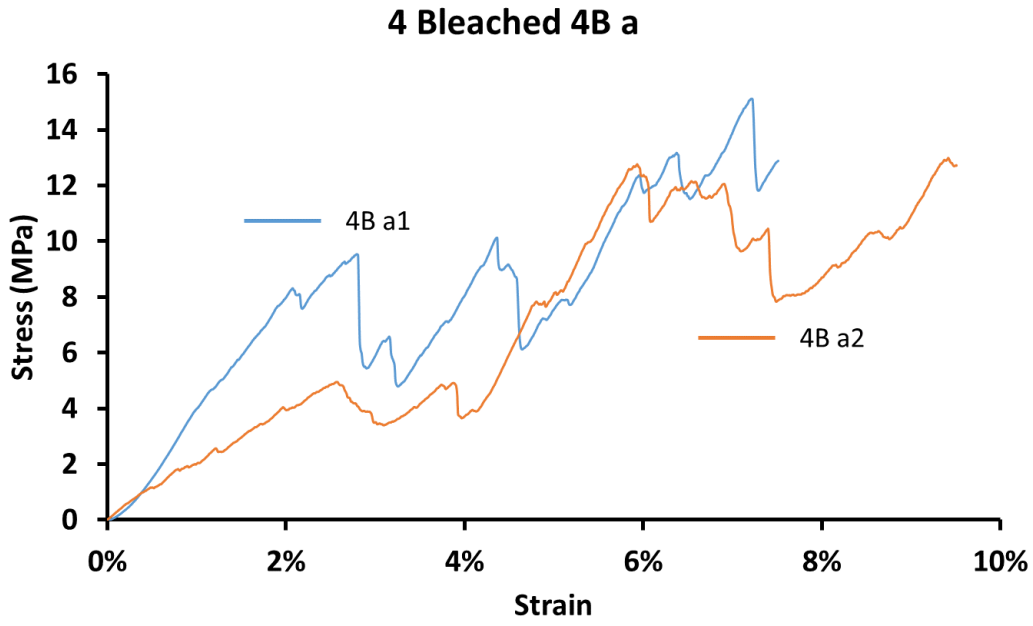

Figure 16. The quasi static result of the 4 Bleached 4B a samples.

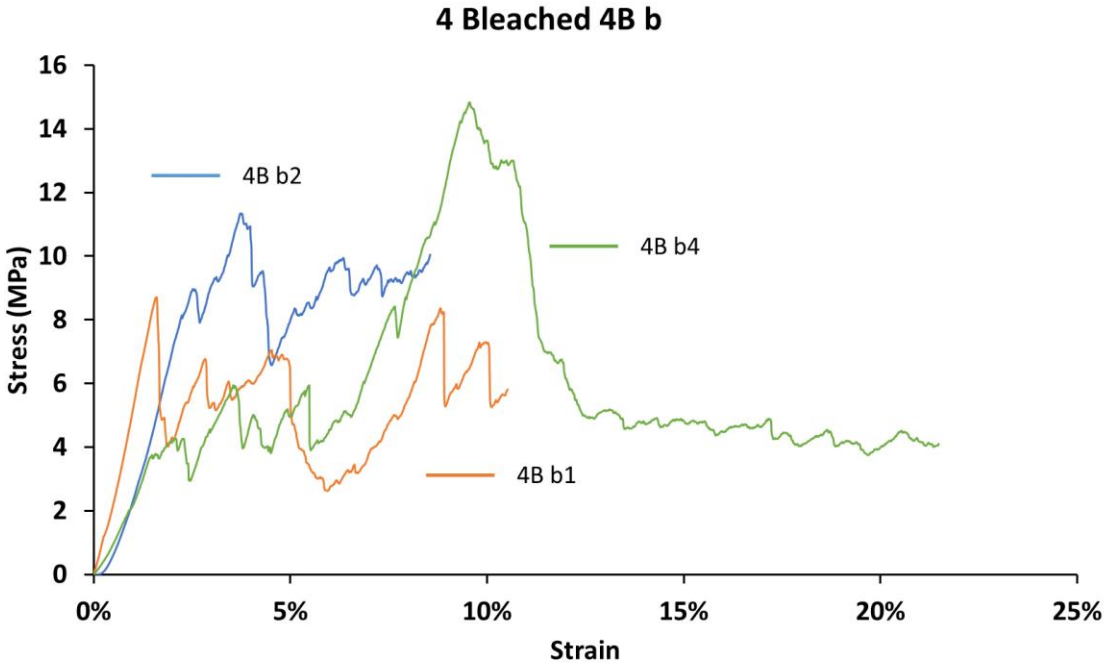

Figure 17. The quasi static result of the 4 Bleached 4B b samples.

3.3 Dynamic Compression Results

The compressive strengths due to the dynamic loading and quasi-static loading are shown in Figure 18 below. There were large variations between the different sample types. These variations are likely due to the irregular cylinder that coral forms, lack of parallelism, and large variations in porosity of each specimen. Several specimens were lost during initial SHPB testing.

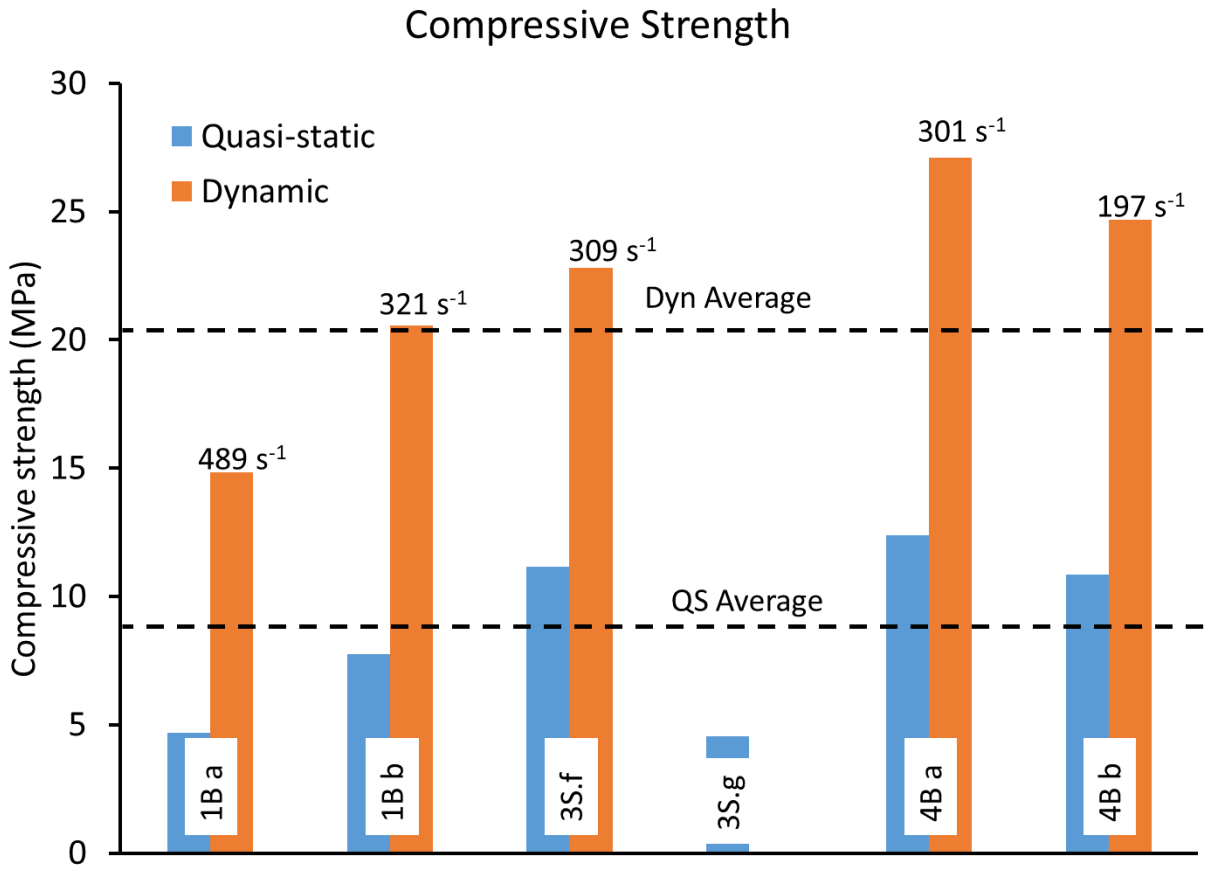

Figure 18. The quasi-static compression with the dynamic compression results. It is difficult to discern if there is a trend due to the lack of parallelism between samples and small sample size.

The stress at failure for the dynamic tests was much higher than the quasi-static results. This is an expected trend in ceramics. The increase in strength is due to inertia effects. The compressive strengths can be seen in Table 3 below.

Table 3. Dynamic compression sample dimensions and results.

Sample	Area (mm^2)	Force (N)	Stress (MPa)	Strain Rates (s^{-1})
1B a	94.23	1407	14.84±2.94	488.5
1B b	66.52	1367	20.55	321.2
3S.f	70.50	1608	22.81	309.3
3S.g		N/A	N/A	N/A
4B a	43.89	1190	27.11	300.8
4B b	44.60	1100	24.68	197.1

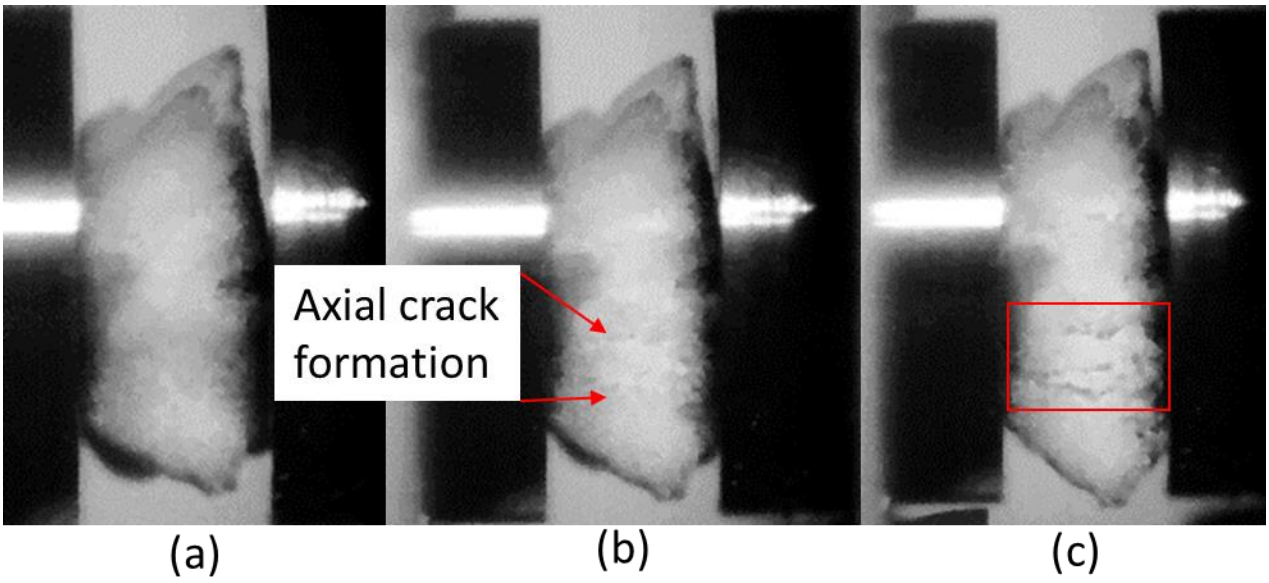

Figure 19. Sample 4B a3 before (a), during (b), and after (c) failure.

Above in Figure 19 the failure of a sample during the dynamic testing can be seen. Cracks form axially during failure. The dynamic and quasi static compression test results can be seen in Table 4.

Table 4. Comparison of quasi static compression and dynamic compression

Sample	Quasi Static Stress (MPa)	Dynamic Stress (MPa)	Difference
1B a	4.68±0.04	14.84±2.94	10.16
1B b	7.76±0.12	20.55	12.79
3S.f	6.26±0.18	22.81	16.55
3S.g	4.55±0.84	N/A	N/A
4B a	7.24±0.38	27.11	19.87
4B b	10.84±2.82	24.68	13.84

4.0 Conclusions and Future Work

This research project revealed that the density and strength of aragonite skeleton from bleached *A. cervicornis* in quasi-static and dynamic loads. The density was found to be 3.13 g/cm^3 which was 8.8% greater than the literature, this may have been caused by residual water in the samples during the He pycnometer tests. One of the samples had its density measured after being cut in half. It is possible that this sample had residual water and oil as the cutting blade was lubricated. It is likely that better sample control would have decreased the standard deviation between the samples.

The dynamic yield strength at 20.80 MPa was found to be an average of 243% higher than that of the quasi-static strength of 8.56 MPa. It might be beneficial to model the coral as a composite since the angles it grows at leads to off axis compressive strength.

Future work that can be done are in situ measurements of coral reefs to measure the loads subjected to coral during regular weather and inclement weather. Future work can also consist of more systematic sample collection to better understand the mechanical properties. Since variability in diameter, porosity, and growth angle occur during growth of *A. cervicornis* a study with rigorous sample extraction and documentation will ensure more accurate results.

5.0 Acknowledgments

This work was funded by the University of Florida University Scholars Program. The author would like to acknowledge Prof. Ghatu Subhash for his guidance and mentorship on this project. The author would also like to acknowledge Naomi Senehi for all her support throughout this project. The author would also like to acknowledge Matthew DeVries, Kshitiz Upadhyay, and Dr. Abir Bhattacharyya for their help in conducting experiments.

6.0 References

[1] Agrawal B., Sharma A. Numerical Investigations of Bio-Inspired Blade Designs to Reduce Broadband Noise in Aircraft Engines and Wind Turbines. Iowa State University Digital repository.

[2] van Nierop, Ernst A. and Alben, Silas and Brenner, Michael P. How Bumps on Whale Flippers Delay Stall: An Aerodynamic Model. Phys. Rev. Lett. Vol 100, Iss 5, pp 054502 1-4. 2008. 10.1103/PhysRevLett.100.054502

[3] Sagrada Familia. 2018. Architecture Sagrada Familia. Fundació Junta Constructora del Temple Expiatori de la Sagrada Família, Barcelona, Spain. http://www.sagradafamilia.org/en/architecture/

[4] Chithra K., Amritha Krishnan K. (2015) BIOTECTURE—A New Framework to Approach Buildings and Structures for Green Campus Design. In: Leal Filho W., Muthu N., Edwin G., Sima M. (eds) Implementing Campus Greening Initiatives. World Sustainability Series. Springer, Cham

[5] Anna-Lena Beger, Manuel Löwer, Jörg Feldhusen, Jürgen Prell, Alexandra Wormit, Björn Usadel, Christoph Kämpfer, Thomas-Benjamin Seiler, Henner Hollert, Franziska Moser, Martin Trautz. Tailored natural components – functional geometry and topology optimization of technical grown plants.

[6] Huang, D., 2012. *Threatened Reef Corals of the World. PLoS ONE 7(3): e34459.http://doi.org/10.1371/journal.pone.0034459. Downloaded on 13 April 2018*

[7] Pandolfi, J.M., R.H. Bradbury, E. Sala, T. P. Hughes, K. A. Bjorndal, R. G. Cooke, D. McArdle, L. McClenachan, M. J. Newman, G. Paredes, and R.R. Warner. 2003. Global trajectories of the long-term decline of coral reef ecosystems. Science, 301: 955-958.

[8] Bellwood, D. R., T. P. Hughes, C. Folke, and M. Nyström. Confronting the coral reef crisis. Nature, 429: 827-833.

[9] Hughes, T. P., N. A. Graham, J. B. Jackson, P. J. Mumby, and R. S. Steneck. 2010. Rising to the challenge of sustaining coral reef resilience. Trends in Ecology & Evolution, 25: 633-642.

[10] Moberg, F., and C. Folke. 1999. Ecological goods and services of coral reef ecosystems. Ecological Economics, 29: 215-233.

[11] Doney, S. C., V. J. Fabry, R. A. Feely, and J. A. Kleypas. 2009. Ocean acidification: the other CO2 problem. Annual Review of Marine Science, 1:169-192. doi: 10.1146/annurev.marine.010908.163834. Downloaded on 05 December 2017.

[12] Barnes, D. T., Coral skeletons: An explanation of their growth and structure, Science, 170, 3964, 1305-1308, 1970.

[13] Gladfelter, E. H., Skeletal development in Acropora cervicornis: I. Patterns of calcium carbonate accretion in the axial corallite, Coral Reefs, 1, 45-51, 1982.

[14] Gladfelter, E. H., Skeletal development in Acropora palmata (Lamarck 1816): a scanning electron microscope (SEM) comparison demonstrating similar mechanisms of skeletal extension in axial versus encrusting growth, Coral Reefs, 26, 883-892, 2007.

[15] Von Euw, S., Zhang, Q., Manichev, V., Murali, N., Gross, J., Feldman, L. C., Gustafsson, T., Flach, C., Mendelsohn, R., Falkowski, P. G., Biological control of aragonite formation in stony corals, Science, 356, 933-938, 2017.

[16] Pandolfi, J.M., R.H. Bradbury, E. Sala, T. P. Hughes, K. A. Bjorndal, R. G. Cooke, D. McArdle, L. McClenachan, M. J. Newman, G. Paredes, and R. R. Warner. 2003. Global trajectories of the long-term decline of coral reef ecosystems. Science, 301: 955-958.

[17] Rude T.J., Strait Jr. L.H., Ruhala L.A., Measurement of Fiber Density by Helium Pycnometry. Journal of Composite Materials, Vol 34, No 22:1948-1959. DOI:10.1106/NUYP-PARA-RA5R-7NUE

[18] A.B. Spierings, M. Schneider, R. Eggenberger, (2011) "Comparison of density measurement techniques for additive manufactured metallic parts", Rapid Prototyping Journal, Vol. 17 Issue: 5, pp.380-386, https://doi.org/10.1108/13552541111156504

[19] Chalker, B., Barnes, D. & Isdale, P. Calibration of x-ray densitometry for the measurement of coral skeletal density Coral Reefs (1985) 4: 95. https://doi.org/10.1007/BF00300867.

[20] Jason T. Cantrell, Sean Rohde, David Damiani, Rishi Gurnani, Luke DiSandro, Josh Anton, Andie Young, Alex Jerez, Douglas Steinbach, Calvin Kroese, Peter G. Ifju, (2017) "Experimental characterization of the mechanical properties of 3D-printed ABS and polycarbonate parts", Rapid Prototyping Journal, Vol. 23 Issue: 4, pp.811-824, https://doi.org/10.1108/RPJ-03-2016-0042

[21] George T. (Rusty) Gray III, 2000. Classic Split-Hopkinson Pressure Bar Testing. ASM Handbook, Vol. 8: Mechanical Testing and Evaluation. P462-476. DOI: 10.1361/asmhba0003296

[22] G. Subhash, G. Ravichandran 2000. Split-Hopkinson Pressure Bar Testing of Ceramics. ASM Handbook, Vol. 8: Mechanical Testing and Evaluation. P497-504. DOI: 10.1361/asmhba0003299

[23] Dusza, J., Fractographic failure analysis of brittle materials, International Journal of Materials and Product Technology, 2003: 15(3), 292-355.

[24] Danzer, R., Mechanical failure of advanced ceramics: The value of fractography, Key Engineering Materials, 2002: 223, 1-18.

[25] Mecholsky, J. J., Passoja, D. E., and Feinberg-Ringel, K. S., Quantitative analysis of brittle fracture surfaces using fractal geometry, Journal of the American Ceramic Society, 1989: 72(1), 60-65.